

First-principles calculations of lattice dynamics in CdTiO₃ and CaTiO₃: Phase stability and ferroelectricity

Hiroki Moriwake,^{1,*} Akihide Kuwabara,¹ Craig A. J. Fisher,¹ Hiroki Taniguchi,² Mitsuru Itoh,² and Isao Tanaka^{1,3}

¹*Nanostructures Research Laboratory, Japan Fine Ceramics Center, Nagoya 456-8587, Japan*

²*Materials and Structure Laboratory, Tokyo Institute of Technology 4259 Nagatsuta, Yokohama 226-8503, Japan*

³*Department of Materials Science and Engineering, Kyoto University, Kyoto 606-8501, Japan*

(Received 6 April 2011; published 9 September 2011)

First-principles calculations of various phases of CdTiO₃ carried out with the aim of obtaining insights into the mechanism of the ferroelectric phase transition and the structure of the low-temperature ferroelectric phase are reported. The results indicate that the preferred symmetry of the low-temperature phase is $Pna2_1$, rather than $P2_1ma$, corresponding to a small relative shift of the Ti and O ions in the paraelectric $Pnma$ phase with the polarization axis parallel to the long axis. Calculated phonon dispersion curves show a distinct soft mode at the Γ point of the $Pnma$ phase, which vanishes in the $Pna2_1$ phase, confirming that the transition to the ferroelectric phase is of the soft-mode displacive type. Calculations of perovskite CaTiO₃, which also has an orthorhombic $Pnma$ structure at room temperature but, unlike CdTiO₃, does not exhibit a ferroelectric phase transition down to 4.2 K, were also carried out to help characterize the factors controlling ferroelectric phase transitions in perovskite titanates.

DOI: [10.1103/PhysRevB.84.104114](https://doi.org/10.1103/PhysRevB.84.104114)

PACS number(s): 77.84.Ek, 77.80.B–

I. INTRODUCTION

Perovskite titanates $ATiO_3$ (where $A = \text{Ca, Sr, Ba, Cd, Pb, or Eu}$) are of immense importance from both a scientific and a practical point of view.^{1–8} They typically undergo a series of phase transitions as a function of temperature and/or pressure; transitions involving spontaneous polarization to form a ferroelectric phase are exploited in a variety of applications, including capacitors, transducers, waveguides, heat sensors, and ferroelectric random access memory.⁹

Cadmium titanate, CdTiO₃, is unusual in that both its paraelectric and ferroelectric phases have orthorhombic structures, whereas for other perovskites exhibiting a ferroelectric phase transition, the paraelectric phase is typically cubic and the ferroelectric phase tetragonal. Under standard conditions, the crystal structure of CdTiO₃ belongs to space group $Pnma$ and can be thought of as being formed by repeated tilting of the TiO₆ octahedral units of the ideal cubic perovskite structure (space group $Pm\bar{3}m$) in a zigzag fashion.¹⁰ This tilting results in a decrease in symmetry and increase in size of the unit cell from one formula unit (5 atoms) for the cubic cell to four formula units (20 atoms) for the orthorhombic cell, as illustrated in Figs. 1(a) and 1(b).

At about 85.5 K, CdTiO₃ undergoes a phase transition from the centrosymmetric orthorhombic structure to a non-centrosymmetric structure.^{11–13} The break in symmetry of the positions of Ti and O ions along the long axis (b axis) and their shift relative to the A cations introduces a dipole moment so that the low-temperature phase is ferroelectric while still retaining overall orthorhombic symmetry. Shan *et al.*¹⁴ performed Rietveld analyses of powder x-ray diffraction data at 15 K and concluded that the ferroelectric structure has either $Pn2_1a$ or $P2_1ma$ symmetry. Both space groups are noncentrosymmetric subgroups of space group $Pnma$. The former corresponds to a softening of the vibrational mode with B_{2u} symmetry in the parent $Pnma$ structure, while the latter results from a softening of the B_{3u} mode.¹⁵

A detailed Raman scattering study by Taniguchi *et al.*¹⁶ revealed that the phase transition is essentially of the ideal displacive type, in which the phonon mode softens toward zero frequency at its Curie temperature, $T_c \sim 85.5$ K. CdTiO₃ thus appears to conform to Cochran's soft-mode model, such that $\omega(\text{TO}) \propto \sqrt{T - T_c}$, where $\omega(\text{TO})$ is the frequency of a transverse optical mode, and T is temperature. In the case of CdTiO₃, the underdamped region extends to less than 0.5 K below T_c ,¹⁶ so CdTiO₃ can be considered a model system for the investigation of ferroelectric phase transitions.

Despite the distinct change in ferroelectric behavior at the Curie temperature, there is still uncertainty regarding the exact space group to which the low-temperature, ferroelectric phase belongs because, unlike other ferroelectrics, the changes in lattice parameters and, hence, the associated atomic displacements are extremely small. Use of polycrystalline samples has also made accurate analysis of the crystal structure difficult.^{13,15,17}

In an attempt to overcome these difficulties, Shan *et al.*¹⁸ carried out single crystal synchrotron x-ray diffraction (XRD) measurements to determine the lattice parameter changes at temperatures above and below T_c to high precision. They reported that a and c parameters remained unchanged before the transition (150 K) and after the transition (70 K), while a slight contraction (0.004 Å) along the b axis was detected. A scatter in values of about ± 0.01 Å was found below 60 K. This slight change in the b parameter most likely represents the limit of their measurements' precision and confirms that the change in lattice parameters at the ferroelectric phase transition of CdTiO₃ is indeed very small. Although they assigned space group $P2_1ma$ to the structure below T_c , in contrast to their initial assignment of $Pn2_1a$ symmetry from measurements on polycrystalline samples,¹⁴ the small structural changes make it difficult to discriminate definitively between the two possible space groups. There is thus still some controversy regarding the precise symmetry of the ferroelectric phase.

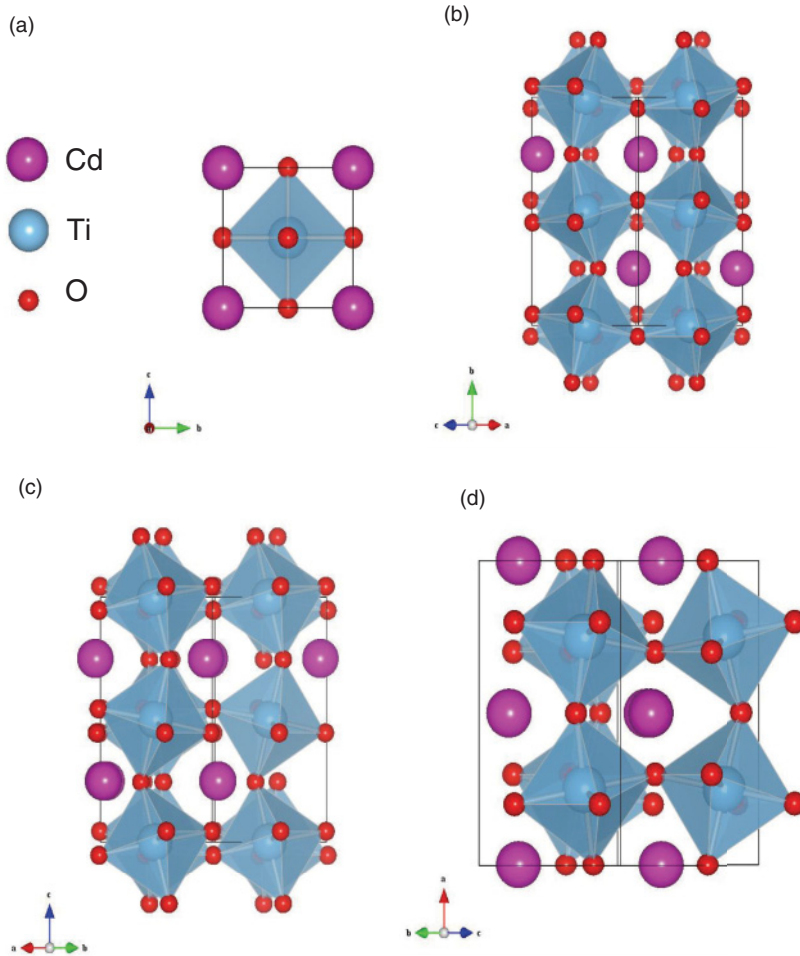


FIG. 1. (Color online) Crystal structures of possible polymorphs of CdTiO_3 : (a) $Pm\bar{3}m$, (b) $Pnma$, (c) $Pna2_1$, and (d) $P2_1ma$ phases.

Gorshunov *et al.*¹⁵ subsequently carried out reflectance and transmittance measurements using IR Fourier spectroscopy on CdTiO_3 single crystals. They found that both B_{2u} and B_{3u} modes soften below the Curie temperature and suggested a multistage transformation sequence from the paraelectric phase to $Pna2_1$ symmetry and finally to $P2_1ma$ symmetry at low temperatures.

Computer simulation offers a powerful means of overcoming the difficulties involved in experimental measurements, allowing the two possible ferroelectric structures to be distinguished on a sound theoretical basis. Indeed, first-principles calculations have been used to examine a large variety of ferroelectric perovskite oxides, including BaTiO_3 ¹⁹ and PbTiO_3 .²⁰ The first theoretical study using density functional theory (DFT) predicted the $Pna2_1$ structure to be unstable compared to the $Pnma$ structure, based on the full-potential linearized augmented plane wave (FLAPW) method.²¹ Lebedev²² later calculated phonon modes at the Γ point of the paraelectric phase, concluding that the $Pna2_1$ phase was the stable form at 0 K. Halilov *et al.*²³ also used DFT to study changes in the stability of the cubic phase as Cd is replaced by Pb. In this study, to shed further light on the phase stability of the various structures, we performed a series of first-principles calculations of the different phases of CdTiO_3 , including a detailed examination of their vibrational modes for a range of wave vectors.

Structures and properties of another titanate, CaTiO_3 , which exists as a paraelectric phase with $Pnma$ symmetry under standard conditions, were also calculated for comparison because of the similarity between the room temperature structures of CaTiO_3 and CdTiO_3 .¹⁰ We have previously shown that under negative pressures CaTiO_3 and CdTiO_3 have similar lattice constants and hence c/a ratios²⁴ for the hypothetical $P4mm$ ferroelectric structure owing to the similarity in ionic radii of Ca^{2+} (1.14 Å) and Cd^{2+} (1.09 Å).²⁵ The key phenomenological difference between them is that, unlike CdTiO_3 , under atmospheric pressure no ferroelectric phase transition is observed for CaTiO_3 , even down to very low temperatures.²⁶

II. METHODOLOGY

First-principles calculations were carried out using the projector-augmented wave (PAW) method²⁷ within DFT, as implemented in the VASP code.^{28,29} The local density approximation (LDA), as proposed by Ceperley and Alder³⁰ and parameterized by Perdew and Zunger,³¹ was used for the exchange-correlation functional. Calculations using the generalized gradient approximation (GGA) with Perdew–Burke–Ernzerhof parameterization³² were also carried out for comparison to reduce the possibility that the calculated properties were artefacts of the particular method used.

Using the PAW method, 3s, 3p, and 4s for Ca; 4d and 5s for Cd; 3s, 3p, 3d, and 4s for Ti; and 2s and 2p electrons for O were treated explicitly as valence electrons. The plane-wave cutoff was set at 600 eV, and the size of the k -point mesh for Brillouin zone sampling of primitive cells, based on the Monkhorst–Pack scheme,³³ was $6 \times 6 \times 6$ for cubic ($Pm\bar{3}m$) cells and $4 \times 3 \times 4$ for orthorhombic ($Pnma$, $Pna2_1$, and $P2_1ma$) cells. Using these parameters, an energy convergence of less than 1 meV per formula unit (f.u.) was achieved. Lattice constants and internal coordinates were fully optimized until residual Hellmann–Feynman (HF) forces were smaller than 1.0×10^{-3} eV/Å while maintaining the symmetry constraints of the given space group.

Dynamical properties were computed from interatomic force constants in real space. The entire set of force constants was obtained from HF forces generated by nonequivalent atomic displacements in a supercell of a given crystal structure. The dimensions of supercells were $2 \times 2 \times 2$ (=40 atoms) for $Pm\bar{3}m$, $2 \times 2 \times 1$ (=80 atoms) for $Pnma$, and $2 \times 1 \times 2$ (=80 atoms) for $Pna2_1$ and $P2_1ma$ systems. For the calculation of HF forces, the k -point mesh sizes of supercells were $3 \times 3 \times 3$ for $Pm\bar{3}m$ and $2 \times 2 \times 2$ for the others. Phonon frequencies were calculated by solving an eigenvalue equation for the dynamical matrix while satisfying sum rules for the lattice constants to maintain translational invariance. All lattice dynamics calculations were performed with the PHONON code.³⁴

In an ionic crystal, dipole-dipole interactions affect interatomic force constants and cause longitudinal optical/transverse optical (LO/TO) splitting when wave vector $k \approx 0$, i.e. near the Γ point. In this study, however, we did not take into account the influence of the dipole on the interatomic force constants, since we are interested primarily in identifying

soft-mode phonons. Inclusion of the LO/TO splitting would have only a slight effect on soft-mode phonons because the dipole-dipole interaction is limited to LO modes when $k \approx 0$, leaving the frequencies of TO modes unchanged.

III. RESULTS AND DISCUSSION

A. Total energies of high- and low-symmetry phases

The calculated lattice parameters for each structure of CdTiO₃ and CaTiO₃ are summarized in Tables I(a) and I(b), respectively, together with previously reported experimental and theoretical data. Our calculations reproduce the experimental lattice parameters well, within the usual LDA error. Rather large errors are found for the $Pm\bar{3}m$ phase of CaTiO₃, but this can be attributed to the fact that the experimental measurements were made at high temperature and thus include a significant thermal expansion component. The energy difference between the orthorhombic and cubic phases of CdTiO₃ is calculated to be $\Delta E = -989$ meV/f.u., in good agreement with previous calculations.²¹ Experimentally, cubic CdTiO₃ has not been observed, consistent with the transition temperature being calculated to exceed the melting point.²¹

In the case of CaTiO₃, which exhibits $Pm\bar{3}m$ symmetry above 1,635 K, the energy difference between the orthorhombic phase and cubic phase is $\Delta E = -410$ meV/f.u. In contrast, for CdTiO₃, the energy differences between the experimentally reported paraelectric phase ($Pnma$) and proposed ferroelectric phases are $\Delta E = -0.23$ meV/f.u. for $Pna2_1$, and $\Delta E = -0.04$ meV/f.u. for $P2_1ma$. These values are very small; the latter close to the uncertainty level of the calculation. Similar energy relations were obtained from GGA calculations, although the errors in the lattice parameters, especially the c

TABLE I. Calculated lattice parameters of (a) CdTiO₃ and (b) CaTiO₃ using LDA compared with previous experimental and theoretical data. Δ is the percentage difference between this work and experimentally determined values.

(a)					
Space group	Lattice parameter	Exp. (Å) ^a	Calc. (Å) ^b	This work (Å)	Δ (%)
$Pm\bar{3}m$	a	–	–	3.809	–
$Pnma$	a	5.403	5.382	5.375	–0.52
	b	7.590	7.574	7.551	–0.52
	c	5.284	5.243	5.248	–0.69
$Pna2_1$	a	5.403	5.378	5.375	–0.52
	b	5.281	5.239	5.247	–0.64
	c	7.583	7.619	7.557	–0.35
(b)					
Space group	Lattice parameter	Exp. (Å) ^c	Calc. (Å) ^d	This work (Å)	Δ (%)
$Pm\bar{3}m$	a	3.8967	–	3.812	–2.16
$Pnma$	a	5.4361	5.412	5.393	–0.79
	b	7.6388	7.537	7.518	–1.58
	c	5.3789	5.290	5.282	–1.80

^aRef. 18.

^bRef. 22.

^cRef. 37.

^dRef. 38.

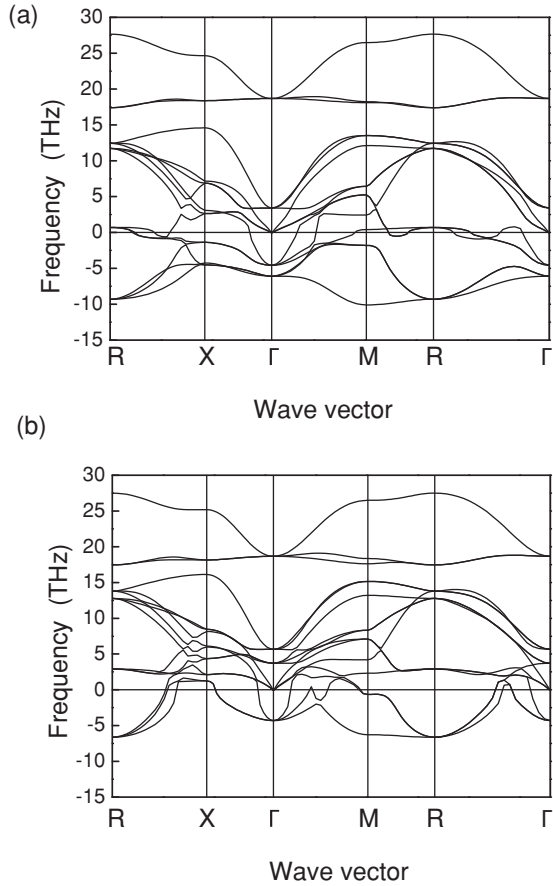


FIG. 2. Phonon dispersion curves for the $Pm\bar{3}m$ phases of (a) $CdTiO_3$ and (b) $CaTiO_3$.

parameter of $Pna2_1$ (+2.99%), are notably worse than for the LDA calculations (Table II).

The small structural and energetic differences between ferroelectric and paraelectric phases of $CdTiO_3$ and $CaTiO_3$ illustrate the difficulty in precisely determining relative phase stabilities from energy calculations alone. In such a situation, accurate phonon dispersion calculations for each structure are indispensable, as they can provide insight into the relative dynamic stabilities of each phase.

B. Soft modes in the cubic phase

Calculated phonon dispersion curves for cubic structures of $CdTiO_3$ and $CaTiO_3$ (space group $Pm\bar{3}m$) are shown in

Fig. 2, with imaginary frequencies plotted on the negative axis. Soft modes occur over a wide range of wave vectors for both compounds, with R and M points exhibiting particularly large imaginary frequencies. The simultaneous condensation of these soft modes corresponds to the cubic-to-orthorhombic phase transition, observed experimentally in the case of $CaTiO_3$ at 1,500 K. These calculated soft-mode features are in good agreement with previous results reported for $CaTiO_3$.^{21,22}

C. Soft modes in the paraelectric orthorhombic phase

Calculated phonon dispersion curves for paraelectric orthorhombic phase of $CdTiO_3$ and $CaTiO_3$ (space group $Pnma$) are shown in Fig. 3. In the case of $CaTiO_3$, the $Pnma$ phase does not exhibit a soft mode for any wave vector. This indicates that the orthorhombic $Pnma$ phase is not only energetically but also dynamically the most stable structure. The paraelectric phase can thus be considered the ground-state structure of $CaTiO_3$. This explains why experimentally no ferroelectric transition has been observed for $CaTiO_3$ down to 0 K at 1 atm. In contrast, the $Pnma$ phase of $CdTiO_3$ exhibits a large soft mode (1.252i THz) at the Γ point. This is the B_{2u} mode, and corresponds to a distortion of the paraelectric orthorhombic (centrosymmetric) structure to the ferroelectric (noncentrosymmetric) orthorhombic structure with $Pna2_1$ symmetry at low temperature.

In an earlier theoretical study of the paraelectric phase of $CdTiO_3$,^{22,35,36} in which phonons were calculated at the Γ point only, another soft mode, smaller in magnitude, was found in addition to the $Pna2_1$ -related mode. The second soft mode was the B_{3u} mode, which corresponds to a transition to $P2_1ma$ symmetry. These two vibrational modes are illustrated in Fig. 4; Fig. 4(a) shows the ionic displacements that take place when the $Pnma$ structure transforms to $Pna2_1$ symmetry and Fig. 4(b) to $P2_1ma$ symmetry. According to our calculations, however, the second mode has a low but real frequency of 0.657 THz. The small energy difference ($\Delta E = -0.04$ meV/f.u.) between the $Pnma$ and $P2_1ma$ phases we obtained is close to the precision of our calculations, but given that the B_{3u} mode has a frequency close to zero, it is unlikely to represent an actual phase transition. Further, by analogy with $SrTiO_3$, Lebedev argued that quantum fluctuations are sufficiently large to suppress lattice distortion associated with this mode.²² This leads us to conclude that the space group for the ferroelectric phase of $CdTiO_3$ is $Pna2_1$, in agreement with the study of Lebedev.²² Since the lattice parameters calculated

TABLE II. Calculated lattice parameters of $CdTiO_3$ using GGA-PBE compared with previous experimental and theoretical data. Δ is the percentage difference between this work and experimentally determined values.

Space group	Lattice parameter	Exp. (\AA) ^a	This work (\AA)	Δ (%)
$Pm\bar{3}m$	a	–	3.888	–
$Pnma$	a	5.403	5.486	1.54
	b	7.59	7.717	1.67
	c	5.284	5.369	1.61
$Pna2_1$	a	5.403	5.492	1.65
	b	5.281	5.359	1.47
	c	7.583	7.810	2.99

^aRef. 18.

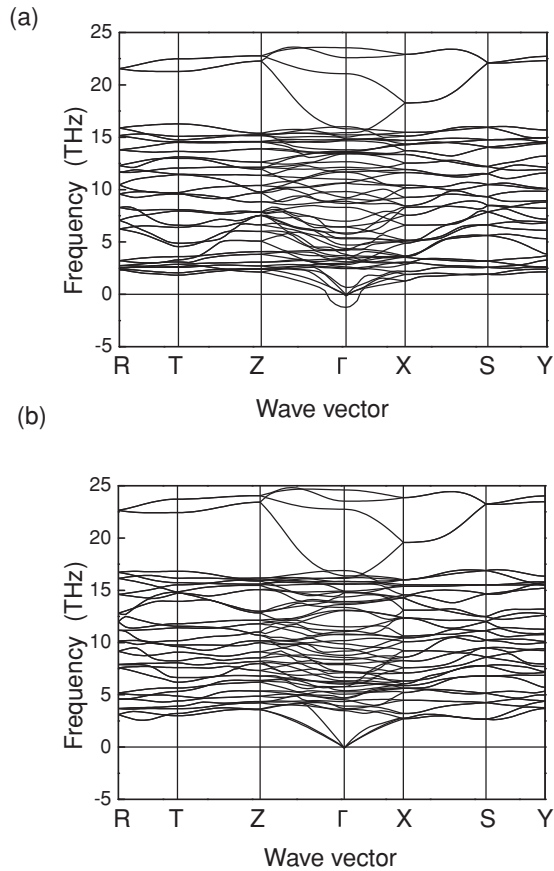


FIG. 3. Phonon dispersion curves for the $Pnma$ phases of (a) CdTiO₃ and (b) CaTiO₃.

in both studies are similar, the difference in the degree of softening of the B_{3u} mode (B_{1u} mode in the $Pbnm$ setting⁹) is probably due to the different pseudopotentials used, Lebedev having used separable nonlocal pseudopotentials generated in-house,^{22,35} whereas we used PAW potentials tested for a range of different Cd-containing compounds by the developers of the VASP code. Our calculated frequency for the B_{2u} mode is approximately one-third that reported by Lebedev,²² indicating

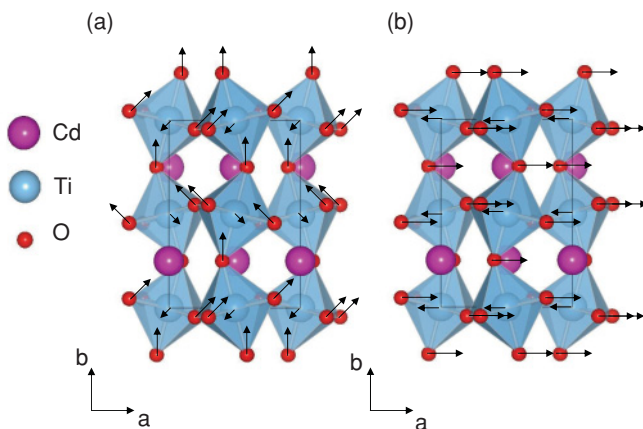


FIG. 4. (Color online) Directions of ion displacements in the $Pnma$ structure corresponding to (a) B_{2u} and (b) B_{3u} modes associated with transformations to the $Pna2_1$ and $P2_1ma$ phases, respectively.

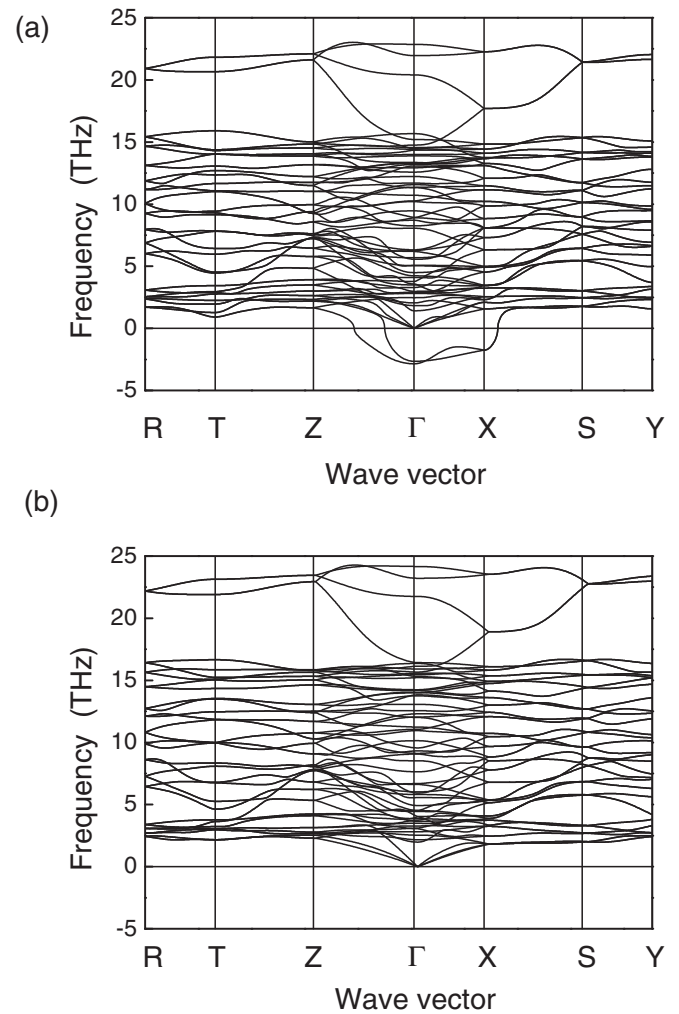


FIG. 5. Phonon dispersion curves for the $Pnma$ phase of CdTiO₃ when the volume is uniformly (a) expanded by 2%, and (b) contracted by 2% relative to the equilibrium value.

that the cation-anion bonds in their structure are less covalent and consequently the structure less rigid.

The ion displacements in the noncentrosymmetric (ferroelectric) $Pna2_1$ structure relative to the centrosymmetric (paraelectric) structure are listed in Table III. Displacements parallel to the a and c axes of the $Pnma$ unit cell conserve centrosymmetry, while those parallel to the b axis lead to a break in centrosymmetry, with Ti and O displaced in opposite directions. This relative displacement is associated with the B_{2u} mode, and is responsible for the spontaneous polarization that makes the $Pna2_1$ phase ferroelectric.

To examine the sensitivity of the phonon behavior on volume, we also performed calculations in which the size of the CdTiO₃ paraelectric unit cell was increased or decreased isotropically by 2% relative to the calculated equilibrium structure. The results are shown in Fig. 5. When the volume is expanded, the B_{2u} and B_{3u} modes both soften significantly, with magnitudes between 2.6i and 2.8i THz. In contrast, when the volume is decreased by 2%, both soft modes vanish. This indicates that the stabilities of the ferroelectric phases of this system are very sensitive to volume. Such behavior helps explain the different symmetries reported from experimental

TABLE III. Ion displacements in ferroelectric CdTiO₃ (*Pna2*₁) relative to positions in the centrosymmetric structure.

Ion	Displacement		
	<i>x</i> (Å)	<i>y</i> (Å)	<i>z</i> (Å)
Cd	±0.001	0	0
Ti	±0.016	+0.005	±0.001
O1	0	-0.030	±0.001
O2	±0.026	-0.035	±0.010

measurements, and indeed the multistage transitions reported by Gorshunov *et al.*,¹⁵ as the experimental conditions in general and state of the sample in particular (e.g. defect concentrations, internal strain, twinning) can easily alter the ferroelectric state.

D. Phonon behavior and structure of the ferroelectric phase

When ions are allowed to relax freely in the directions corresponding to the B_{2u} soft mode at the Γ point [Fig. 4(a)], structural optimization of the *Pnma* phase of CdTiO₃ results in a transformation to the ferroelectric *Pna2*₁ phase, a further indication of the greater stability of this phase compared to the *P2*₁*ma* phase. Lattice parameters of the resulting ferroelectric phase are listed in Table I and internal coordinates in Table IV. The change in lattice parameters during the transition is very small. According to our calculations, the difference in lattice parameters between the paraelectric and ferroelectric phases is 0.00% for the *a* parameter, +0.07% for the *b* parameter, and -0.01% for the *c* parameter (relative to the *Pnma* structure). These results are in very good agreement with the measurements of Shan *et al.*¹⁸

Our calculations show that, concomitant with the slight structural change at the transition, the energy difference between the two phases is also very small. As noted in Sec. III A, the ferroelectric (*Pna2*₁) phase is energetically more stable than the paraelectric (*Pnma*) phase by only $\Delta E = -0.23$ meV/f.u. The same energy difference was

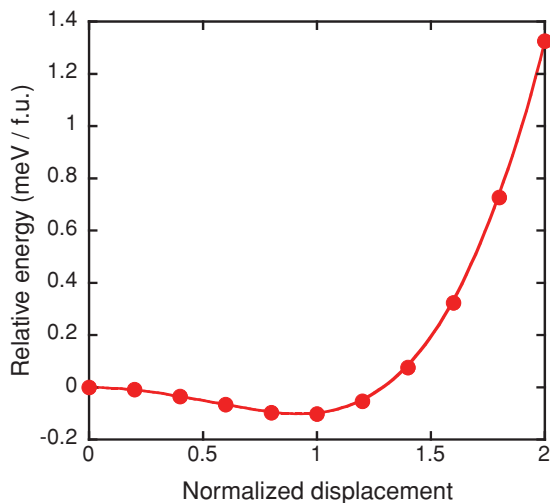


FIG. 6. (Color online) Change in energy as a function of ion displacement for the B_{2u} mode in the *Pnma* structure. The displacement has been normalized to the atomic positions of the polar (*Pna2*₁) structure.

obtained using dense *k*-point meshes from $4 \times 3 \times 4$ up to $8 \times 6 \times 8$ for both *Pnma* and *Pna2*₁ phases. The minuteness of this difference can be appreciated by comparing it with energy changes reported for ferroelectric transitions in other systems, e.g. $\Delta E = -6$ meV/f.u. at $T_c = 400$ K for *Pm* $\bar{3}m$ to *P4mm* in BaTiO₃, and $\Delta E = -44$ meV/f.u. at $T_c = 763$ K in PbTiO₃, both of which have higher Curie temperatures than CdTiO₃.

Given that the energy difference between the paraelectric and ferroelectric phases is extremely small, we also calculated the energy change on displacing the ions along B_{2u} soft mode, assuming the same lattice parameters as for the paraelectric phase. The results are shown in Fig. 6, where the horizontal axis is the displacement normalized by the atomic positions in the polar structure, and the vertical axis is the energy change. Although the energy gain is very small (-0.10 meV/f.u.), it is sufficient to stabilize the ferroelectric structure. Roughly half of the energy gain between the paraelectric *Pnma* phase and ferroelectric *Pna2*₁ phase can thus be attributed to polarization of the structure. The remainder results from relaxation of the lattice to accommodate this change, as expressed in the small change in lattice volume.

Treating the polarization as a Berry phase, a value of 0.10 C/m² is obtained for the spontaneous polarization of CdTiO₃. This is smaller than the value calculated by Lebedev,²² but still approximately one to two orders of magnitude larger than the values of 0.002 C/m² (Ref. 14) and 0.009 C/m² (Ref. 36) reported for polycrystalline samples. We note that the polarization-electric (*P-E*) field hysteresis curves reported from experiment were not sufficiently saturated; higher saturation levels should result in higher polarization values being obtained.

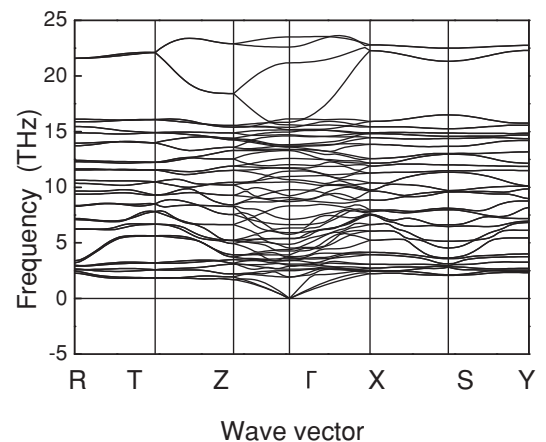


FIG. 7. Phonon dispersion curves for the ferroelectric *Pna2*₁ phase of CdTiO₃.

TABLE IV. Optimized coordinates of ions in the ferroelectric phase (space group $Pna2_1$) of CdTiO_3 . Experimental values from Ref. 14 are given in parentheses.

Ion	Fractional coordinates		
	x	y	z
Cd	0.4569 (0.4593)	0.9899 (0.9917)	0.25 (0.25)
Ti	0.5029 (0.507)	0.4998 (0.496)	0.0006 (0.004)
O1	0.0303 (0.027)	0.0934 (0.091)	0.246 (0.241)
O2	0.8031 (0.808)	0.3033 (0.277)	0.5445 (0.547)
O3	0.7066 (0.701)	0.7993 (0.823)	0.4466 (0.545)

Born effective charges along the polar direction (c axis of the $Pna2_1$ phase) were calculated to be +2.63 for Cd, +6.88 for Ti, -5.42 for O1, -1.99 for O2, and -2.00 for O3 (where O1 is O ion bonded to Ti along the c axis). The large Born effective charges of the cations compared to their formal charges is a typical phenomenon of titanate perovskites and can be ascribed primarily to the covalent bonding between Ti-3d and O-2p orbitals.

The calculated phonon dispersion curve for the $Pna2_1$ phase of CdTiO_3 is shown in Fig. 7. In this ferroelectric phase, no imaginary phonon branch is found for any wave vector. This indicates that the $Pna2_1$ phase is not only energetically stable but also dynamically stable. This suggests that the $Pna2_1$ phase represents the most stable structure of CdTiO_3 down to absolute zero with no further ferroelectric phase transition below T_c . It is possible that assignment of space group $P2_1ma$ to ferroelectric CdTiO_3 based on synchrotron XRD of single crystals in earlier work¹⁸ was because the atom displacements were at the limit of the precision of the measurement apparatus; our calculations suggest that the B_{3u} soft mode necessary for the paraelectric phase to transform to $P2_1ma$ symmetry is nonexistent or at least very weak. However, given the small changes in energy involved and the strong dependence of ferroelectric transitions on pressure, higher-precision experimental measurements will be required to confirm that the stable ferroelectric phase of CdTiO_3 down to zero K maintains its $Pna2_1$ symmetry.

IV. CONCLUSIONS

We have performed a series of first-principles calculations of CdTiO_3 and CaTiO_3 in order to characterize in detail their phase transition sequences and determine the likely structure of the former compound's low-temperature, ferroelectric form. The results indicate that the paraelectric orthorhombic phase will transform to a ferroelectric phase with $Pna2_1$ symmetry with the polarization axis (c axis) parallel to the b axis of the paraelectric orthorhombic phase within the $Pnma$ setting, in good agreement with experiment. Further, there appears to be no additional ferroelectric phase between the $Pna2_1$ phase and absolute zero, although the appearance of soft modes associated with ferroelectric transitions are shown to be highly sensitive to the amount of lattice strain. In contrast, in the case of CaTiO_3 , soft modes are found in the phonon dispersion curves of the cubic phase but not in the $Pnma$ phase, confirming that this is the ground state structure, in agreement with experiment.

ACKNOWLEDGMENTS

The authors thank David J. Singh at Oak Ridge National Laboratory for useful discussions. This work was supported by the Ministry of Education, Culture, Sports, Science, and Technology of Japan through the Grants-in-Aid for Priority Area "Atomic Scale Modification" (No. 474) and Scientific Research (C) (No.21560708).

*moriwake@jfcc.or.jp

¹G. Burns and B. A. Scott, *Phys. Rev. B* **7**, 3088 (1973).

²G. Burns, *Phys. Rev. B* **10**, 1951 (1974).

³G. Burns and F. H. Dacol, *Phys. Rev. B* **18**, 5750 (1978).

⁴H. P. Soon, H. Taniguchi, Y. Fujii, M. Tachibana, and M. Itoh, *Phys. Rev. B* **78**, 172103 (2008).

⁵H. Taniguchi, M. Takesada, M. Itoh, and T. Yagi, *Phys. Rev. B* **72**, 064111 (2005).

⁶M. Takesada, M. Itoh, and T. Yagi, *Phys. Rev. Lett.* **96**, 227602 (2006).

⁷T. Shigenari, K. Abe, T. Takemoto, O. Sanaka, T. Akaike, Y. Sakai, R. Wang, and M. Itoh, *Phys. Rev. B* **74**, 174121 (2006).

⁸H. Taniguchi, M. Itoh, and T. Yagi, *Phys. Rev. Lett.* **99**, 017602 (2007).

⁹K. M. Rabe, M. Dawber, C. Lichtensteiger, C. H. Ahn, and J. M. Triscone, in *Physics of Ferroelectrics: A Modern Perspective*, edited

by K. M. Rabe, C. H. Ahn, and J. M. Triscone (Springer, Berlin, 2007), p. 20.

¹⁰S. Sasaki, C. T. Prewitt, J. D. Bass, and W. A. Schulze, *Acta Crystallogr. C* **43**, 1668 (1987).

¹¹G. A. Smolenski, *Dokl. Akad. Nauk. SSSR* **70**, 405 (1950).

¹²H. El-Mallah, B. E. Watts, and B. Wanklyn, *Phase Trans.* **9**, 235 (1987).

¹³P. H. Sun, T. Nakamura, Y. J. Shan, Y. Inaguma, and M. Itoh, *Ferroelectrics* **217**, 137 (1998).

¹⁴Y. J. Shan, H. Mori, R. Wang, W. Luan, H. Imoto, M. Itoh, and T. Nakamura, *Ferroelectrics* **259**, 85 (2001).

¹⁵B. P. Gorshunov, A. V. Pronin, I. Kutskov, A. A. Volkov, V. V. Lemanov, and V. I. Torgashev, *Phys. Solid State* **47**, 547 (2005).

¹⁶H. Taniguchi, Y. J. Shan, H. Mori, and M. Itoh, *Phys. Rev. B* **76**, 212103 (2007).

- ¹⁷Y. J. Shan, H. Mori, K. Tezuka, H. Imoto, and M. Itoh, *Ferroelectrics* **270**, 381 (2002).
- ¹⁸Y. J. Shan, H. Mori, K. Tezuka, H. Imoto, and M. Itoh, *Ferroelectrics* **284**, 107 (2003).
- ¹⁹R. D. King-Smith and D. Vanderbilt, *Phys. Rev. B* **49**, 5828 (1994).
- ²⁰G. Saghi-Szabo, R. E. Cohen, and H. Krakauer, *Phys. Rev. B* **59**, 12771 (1999).
- ²¹G. Fabricius and A. L. García, *Phys. Rev. B* **66**, 233106 (2002).
- ²²A. I. Lebedev, *Phys. Solid State* **51**, 802 (2009).
- ²³S. V. Halilov, M. Fornari, and D. J. Singh, *Appl. Phys. Lett.* **81**, 3443 (2002).
- ²⁴H. Moriwake, Y. Koyama, K. Matsunaga, T. Hirayama, and I. Tanaka, *J. Phys. Condens. Matter* **20**, 345207 (2008).
- ²⁵R. D. Shannon, *Acta Cryst. A* **32**, 751 (1976).
- ²⁶V. V. Lemanov, A. V. Sotnikov, E. P. Smirnova, M. Weihnacht, and R. Kunze, *Solid State Commun.* **110**, 611 (1999).
- ²⁷P. E. Blöchl, *Phys. Rev. B* **50**, 17953 (1994).
- ²⁸G. Kresse and J. Furthmüller, *Phys. Rev. B* **54**, 11169 (1996).
- ²⁹G. Kresse and J. Furthmüller, *Comput. Mater. Sci.* **6**, 15 (1996).
- ³⁰D. M. Ceperley and B. J. Alder, *Phys. Rev. Lett.* **45**, 566 (1980).
- ³¹J. P. Perdew and A. Zunger, *Phys. Rev. B* **23**, 5048 (1981).
- ³²J. P. Perdew, K. Burke, and M. Ernzerhof, *Phys. Rev. Lett.* **77**, 3865 (1996).
- ³³H. J. Monkhorst and J. D. Pack, *Phys. Rev. B* **13**, 5188 (1976).
- ³⁴K. Parlinski, Y. Kawazoe, and Y. Waseda, *J. Chem. Phys.* **114**, 2395 (2001).
- ³⁵A. I. Lebedev, *Phys. Solid State* **51**, 362 (2009).
- ³⁶M. E. Guzhva, V. V. Lemanov, and P. A. Markovin, *Phys. Solid State* **43**, 2146 (2001).
- ³⁷R. Ali and M. Yashima, *J. Solid State Chem.* **178**, 2867 (2005).
- ³⁸E. Cockayne and B. P. Burton, *Phys. Rev. B* **62**, 3735 (2000).
- ³⁹All crystal structure figures are drawn by software package *VESTA*, K. Momma and F. Izumi, *J. Appl. Crystallogr.* **41**, 653 (2008).